Ocean Engineering 301 (2024) 117543

Contents lists available at ScienceDirect

Ocean Engineering

journal homepage: www.elsevier.com/locate/oceaneng

Research paper

A new numerical modelling framework for fixed oscillating water column wave energy conversion device combining BEM and CFD methods: Validation with experiments

Vaibhav Raghavan [a,*], Irene Simonetti [b], Andrei V. Metrikine [a], George Lavidas [a], Lorenzo Cappietti [b]

[a] Delft University of Technology, Stevinweg 1, Delft, 2628 CN, Zuid Holland, Netherlands
[b] LABIMA, University of Florence, Piazza di San Marco 4, Florence, 50121, Firenze, Italy

ARTICLE INFO

Keywords:
Oscillating water column
CFD
BEM
HAMS-MREL
OpenFOAM
Framework

ABSTRACT

The Oscillating Water Column (OWC) wave energy converter has been shown to have high potential, thus rendering extensive development in recent years. In order to further accelerate its development, highly accurate yet computationally efficient tools are necessary particularly when studying the interaction of multiple OWC devices. This paper proposes a new framework for fixed OWC devices with an orifice, that uses the input from a high fidelity non-linear numerical model to improve the accuracy of a low fidelity linear numerical model keeping computational costs low. This is done by accounting for the non-linearities in the pressure-flow of an orifice in the input to the linear numerical model. Experimental data is used to validate the framework, thus providing an accurate and computationally efficient linear numerical model, that can be used for the preliminary analysis of fixed OWC devices.

1. Introduction

In the process of energy transition towards zero-carbon, the conversion of wave energy may play an important role, contributing to the climate neutrality of the energy supply. The convergence to commercial level for Wave Energy Converters (WECs) is currently slowed down by some technical and non-technical barriers, e.g., the need to reduce the Levelized Cost of Energy (LCOE) and to increase the expected survivability of WECs under extreme waves. To overcome these barriers, accurate and not-computationally demanding numerical tools to model the device behaviour are needed, both to perform optimization studies and to derive key performance indicators, which are in turn fundamental drivers of the sector development towards commercial maturity.

Among the different technologies for wave energy conversion proposed over the years (Zhang et al., 2021), the OWC is largely considered as one of the technologies with the highest potential (Falcão and Henriques, 2016). The OWC has the advantage of simplicity, utilization of off-the-shelve components, and robust design for Power Take Off (PTO) system i.e. self-rectifying air turbines (Falcão et al., 2018). Furthermore, the PTO can achieve high rotational speeds, which implies lower torques and stresses compared to other devices to generate comparable power (Rosati et al., 2022).

In its fixed version, the OWC consists of a hydraulic structure, a hollow caisson made of concrete or steel, open underwater for the interaction with the incident waves, and an upstaging air chamber connected to a duct embedding an air turbine. The sea waves cause an oscillating heave motion of the inner column of water in the caisson, alternatively compressing and expanding the upstanding air, driving an airflow through the turbine.

There are many numerical methods currently available for modelling OWCs. These range from low-fidelity models such as Boundary Element Method (BEM) to high-fidelity models such as those based on Computational Fluid Dynamics (CFD). The work of Rosati et al. (2022) provides a comprehensive overview of the numerical modelling and control of OWCs for low to mid-fidelity models. Within the linear hydrodynamic models, two approaches are most popular - (1) Piston method, where free surface above the water column is treated as a neutrally buoyant piston which is characterized by added mass, radiation damping and excitation forces (Evans, 1978). (2) Uniform pressure method, which assumes a uniformly distributed pressure on the inner free surface allowing the free surface to deform (Evans, 1982).

WAMIT, the most popular commercial BEM solver for OWCs accommodates both these methods. Within the piston method, WAMIT offers

* Corresponding author.
E-mail address: v.raghavan@tudelft.nl (V. Raghavan).

https://doi.org/10.1016/j.oceaneng.2024.117543
Received 6 December 2023; Received in revised form 5 March 2024; Accepted 15 March 2024
Available online 20 March 2024

the two-body approach and the generalized modes approach. In the two body approach, the first body is the hull of the OWC and the second body is the piston. With the generalized modes approach, the piston can be modelled as a thin massless disk above the free surface moving in specific modes, with the heave mode generally being the most important for OWCs (Delauré and Lewis, 2003, Bingham et al., 2015). When considering mid-fidelity models, the time-domain hydrodynamic models based on Cummin's equation utilizing convolution integrals are very popular. These utilize frequency domain coefficients as input from models such as BEM.

The air chamber and turbine/generator play a vital role in the dynamics of an OWC system. The hydrodynamic models are coupled to frequency/time-domain models for the air chamber, based on the mass balance equation, and most often consider the isentropic condition to model the thermodynamics in the air chamber (Sarmento et al., 1990; Falcão et al., 2022, Belibassakis et al., 2020). Furthermore, the turbine/generator model is added which is either an air turbine (Maeda et al., 1999) or an electric generator (Abad et al., 2011).

In the past years, the high computational time of high-fidelity, fully nonlinear models based on Computational Fluid Dynamics (CFD) as compared to BEM-based approaches strongly limited their diffusion for simulating OWC devices. However, the continuous increase in the availability and performance of high-performance computing has increased use of CFD for OWCs and WECs in general (Penalba et al., 2017). The CFD approach allows for studying the hydrodynamic interaction between the device and the incident waves accounting for multi-phase, real fluid and nonlinear effects. In particular, energy losses due to viscous dissipation through the PTO and flow separation with vortices formation at the OWC front wall have been often observed (e.g., Zhang et al., 2012, Huang et al., 2020, López et al., 2015).

Processes in the air chamber during a wave cycle may be highly non-linear, resulting in possible errors in the estimation of the differential air pressure when using linear models (Sykes R.K., 2011). Both two-dimensional (Deng et al., 2019; Gaspar et al., 2020; Simonetti and Cappietti, 2021) or three-dimensional (Iturrioz et al., 2015; Simonetti et al., 2018; Shalby et al., 2019) CFD-based Numerical Wave Tanks (NWT) for simulating OWC devices have been developed and validated, showing relative errors on free surface oscillation and air pressure in the OWC chamber within a range of ±5%–15% compared to laboratory tests. Most of the CFD-NWTs for OWC devices are based on solving Reynolds-averaged Navier–Stokes equations with the k-epsilon or k-omega turbulence models (as recently reviewed in Opoku et al. (2023)), while the use of Large Eddy Simulations is more limited (e.g. Simonetti et al., 2017; Carlo et al., 2023), due to the higher computational demands.

BEM models to simulate OWC devices equipped with a linear turbine in the frequency domain have been often used in the literature, while the use of BEM to reproduce OWC with non-linear PTO is less common. Sarmento et al. (1990), Fox et al. (2021) modelled the linear turbine based on the mass transport equation considering air compressibility which results in a coefficient relating the pressure to the discharge (also referred to as the flow rate). Since the imaginary part essentially has a restoring effect, it is regarded as a spring in the system (Sheng and Aggidis, 2022). This is attributed to the air compressibility. Belibassakis et al. (2020) obtained a similar relation, within the BEM formulation considering variable bathymetry, using the mass transport equation in combination with the isentropic thermodynamic condition (simplification to the air compressibility effect (Malara and Arena, 2013) occurring above the water column surface leading to a complex coefficient relating pressure above the water column and air discharge through the Wells turbine.

The low-fidelity models such as BEM are based on linear potential flow theory, that consider the fluid as inviscid and irrotational. This allows the wave fields due to the fluid structure interaction, to be computed using velocity potentials which are linearly superimposed. These methods are thus incapable of modelling non-linear and turbulent phenomena. Considering non-linear phenomena within low-fidelity models can be of importance as it improves their fidelity while keeping computational costs low.

The current research therefore proposes a new framework that combines the high-fidelity and low-fidelity models for OWCs. A fixed bottom-detached box OWC is used as a case study and will henceforth be referred to as the box model. The box model has an orifice, which introduces a quadratic flow-pressure relationship (Falcão et al., 2022), and is representative of the behaviour of an impulse turbine. The motivation for the use of the orifice was to add non-linearity within the OWC system, and check how to best capture it with a linearized numerical model. While previous works have been done to improve the performance for low fidelity models using experimental data (Falcão et al., 2022, Raghavan et al., 2023), using this procedure consistently is difficult. This is because setting up and performing experiments is a very costly and time-consuming process and replicating experiments does not guarantee similar results, since the conditions have to be replicated in the exact way which is very difficult to do. Therefore in the current work, using the input obtained from a CFD-NWT modelled using the VOF approach in OpenFOAM, a BEM model derived in HAMS-MREL (in-house multiple body BEM solver of TU Delft; under review at 'Applied Ocean Energy Research'. This solver is built upon the HAMS solver described in (Liu, 2019)) is improved and validated against experimental data. The proposed framework would allow OWCs to be modelled as both single devices as well as in arrays, giving an accurate preliminary estimate while keeping computational costs low.

The paper is structured as follows. First, the experimental study is explained in Section 2. This is followed by the descriptions of the CFD model, the BEM model and the framework combining BEM and CFD in Section 3 showcasing two CFD-BEM models. The main results are discussed in Section 4, following by the conclusions and future work discussion in Section 5.

2. Experiments

This section discusses the experimental setup and procedure that is used for validation of the CFD model as well as the BEM-CFD framework introduced in the next section.

2.1. Experimental setup

The box experimental model was installed in the Wave-Current flume One (LABIMA-WCF1) located at LABIMA, University of Florence, Italy. The LABIMA-WCF1 is a structure built entirely from steel and glass side walls, with a total length of 37.0 m and width and height of 0.8 m. The piston type wave generator is installed at one end of the wave flume, and it has a stroke equal to 1.5 m, driven by an electromechanical system with an absolute encoder of 0.01 cm accuracy of piston (Kisacik et al., 2020).

The Box model has a height of 0.527 m, length (orthogonal the wave direction) of 0.795 m, and width (along the wave direction) of 0.256 m. The plan and elevation of the model are shown in Fig. 1(a) and the device as placed in the wave tank is shown in Fig. 1(b). The OWC model was tested on a horizontal bottom in 0.5 m water depths. The horizontal distance between the wave generator and the OWC model is 18 m, which is close to the centre of the tank. This distance was deemed sufficient to propagate the selected cases of regular waves at the model location. The length was kept almost equal to the WCF1 width to set-up a fully 2D modelling thus avoiding the generation of transverse wave fields (e.g. wave reflection from the flume side walls). A slit of approximately 1.7 mm was created at the top of the Box model to function as an orifice. The size of the slit $V = 1.7$ mm can be justified by the fact that we know, from previous studies (Simonetti et al., 2017, 2016), that the optimal damping for the OWC chamber is for ratios of the slot area (A_v) to the top cover area (A_v), in the range of 1 to 2%.

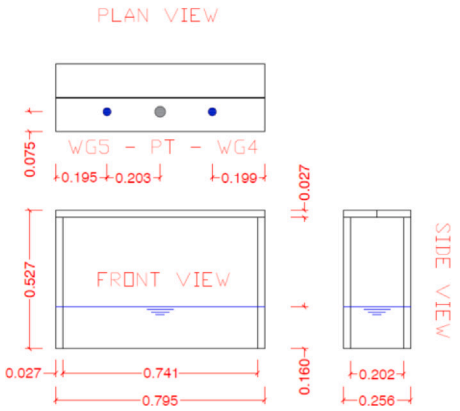

(a) Box OWC device plan and elevations

(b) Box OWC placed in tank - WG4 and WG5 are wave gauge designated by orange wires and PT is the pressure gauge depicted by the black wire

Fig. 1. Box OWC device (Raghavan et al., 2022).

With the dimensions currently utilized for the model, the ratio A_v/A_t is approximately 1%, which is in the optimal range. The internal width of 0.2 m for the water column was so chosen to be within 30% of the minimum wavelength of the generated waves, thus allowing the internal free surface to oscillate almost completely in heave motion. This is motivated by the need to avoid sloshing phenomena in the OWC chamber, which may be relevant when the ratio of the OWC internal width to the incident wavelength increases. Literature suggests that values of such a ratio exceeding approximately 1 to 4 should be avoided as discussed, e.g., in W. Sheng and Alcorn (2012).

The Box model was firmly fixed to the side walls such that the internal draft was 0.16 m. In Fig. 1(a), WG4 and WG5 refer to the wave gauges used to measure the displacement of the internal free surface with respect to the still water level inside, and PT is the pressure sensor used to measure the pressure fluctuations in the air pocket above the internal free surface. Two wave gauges were chosen to be used for the model to ensure there was no sloshing of the internal water column.

Two test configurations were utilized. The first configuration was without the OWC model. This configuration was used to measure the testing wave conditions at the model location, in the absence of wave-structure interaction, which would later be used to test the OWC model. The second configuration was with the device installed.

2.2. Experimental procedure

The test cases selected for the experiment were based on the Le Méhauté diagram (shown in Fig. 2), which shows the regions of applicability of the various wave conditions (i.e. linear and non-linear) for regular waves based on the water depth (h), wave height(H), wave length(λ) and time period (τ) of the wave.

10 regular wave cases were considered for this (see Table 1). The first four tests H01–H04 were performed to compare how BEM and CFD performed with various wave theories (Airy wave theory, Stoke's 2^{nd} order and Stoke's 3^{rd} order) and cases H03, H05–10 were done keeping the wave height almost constant and varying the time period of the incident waves. This was to determine the Response Amplitude Operator (RAO) for the water column in the device under different wave steepness.

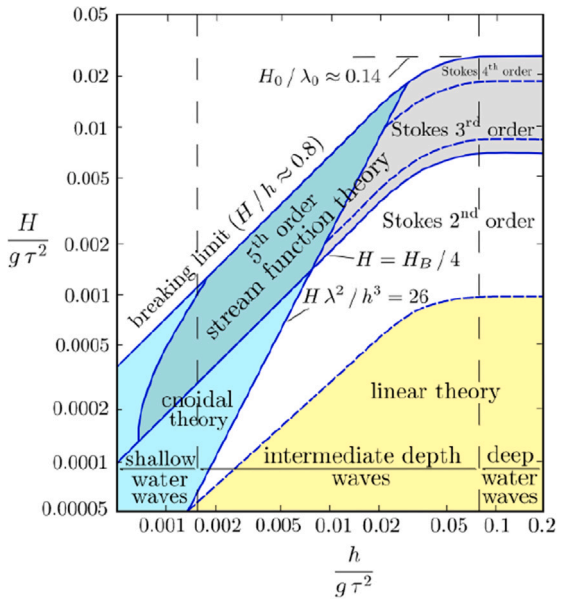

Fig. 2. Le Méhauté diagram (Le Méhauté, 1976).

The input for the wave maker was provided as an exponentially increasing sinusoidal curve starting from 0 to the desired wave height. As an example, the generated input conditions are shown in Fig. 3 for case H01. This was performed for all 10 cases. The number of waves generated by the wave maker was selected to obtain a time window during which a fully developed wave field at model location was present in absence of the reflected wave fields coming for the two flume ends. Fig. 4 shows the displacement as measured by the wave gauges WG4 and WG5 for the case H02.

The periods within the red box indicate the time period when the generated waves from the piston pass WG4/WG5 in the absence of the reflected waves coming from the end of the flume (indicated in Fig. 4). The constructive interference between the incident and reflected waves can be observed in the green box (indicated in Fig. 4).

Table 1
Test Matrix — effective values measured at the model position by means of tests in absence of the model (water depth is 0.5 m).

Case name	Wave height, H (cm)	Wave period measured, τ (s)	Wave frequency, ω (rad/s)	Water steepness, H/L (-)	Wave theory
H01	2.50	2.34	2.68	0.050	Airy linear
H02	1.10	1.43	4.39	0.022	Airy linear
H03	6.60	1.43	4.39	0.132	Stokes 2^{nd} order
H04	9.30	1.43	4.39	0.186	Stokes 3^{rd} order
H05	6.30	1.00	6.28	0.126	Stokes 3^{rd} order
H06	6.40	1.20	5.23	0.128	Stokes 3^{rd} order
H07	6.50	1.60	3.93	0.130	Stokes 3^{rd} order
H08	6.00	1.80	3.49	0.120	Stokes 2^{nd} order
H09	6.10	2.00	3.14	0.122	Stokes 2^{nd} order
H10	6.10	2.20	2.85	0.122	Stokes 2^{nd} order

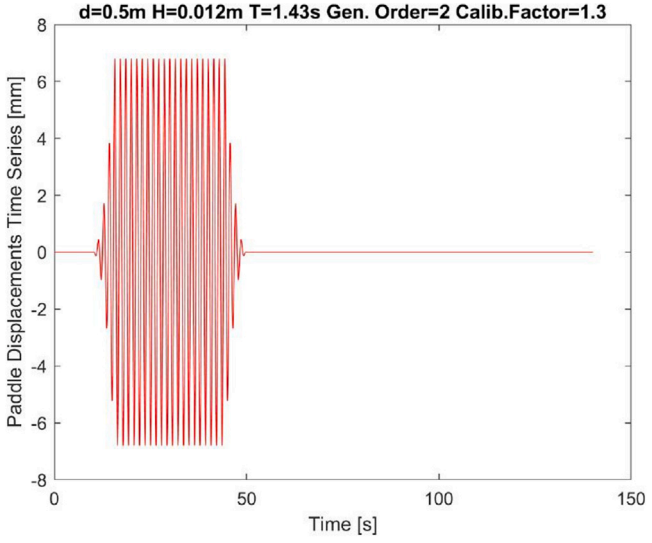

Fig. 3. Input for test case H02 to wavemaker.

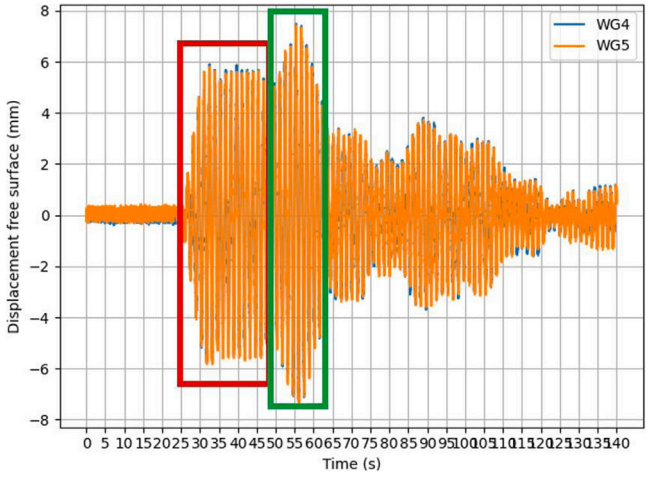

Fig. 4. Displacements of the free surface measured by wave gauges WG4 and WG5 for the case H02. Red box: the incident waves. Green box: Interference of incident and reflected waves.

The displacements of WG4 and WG5 within the red box (indicated in Fig. 4) are used to calculate the mean wave height and air discharge for each case. A similar procedure as for WG4 and WG5 was used for PT to obtain the mean air pressure fluctuations. The pressure fluctuation for case H02 is shown in Fig. 5.

3. Methodology

This section provides a description of the CFD-NWT and numerical BEM model of the Box OWC device, followed by the framework that

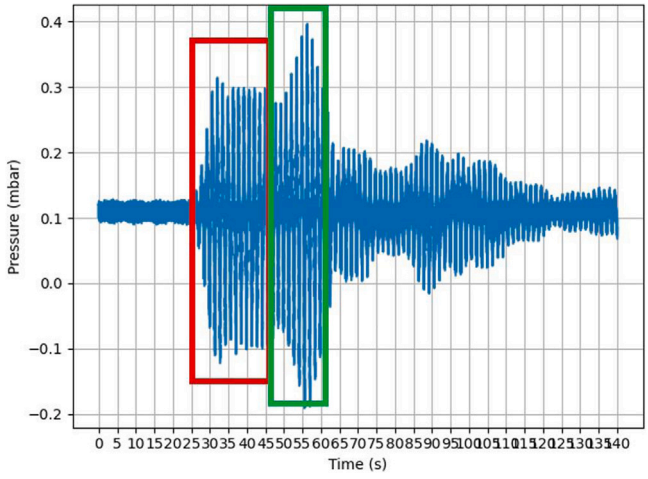

Fig. 5. Pressure measurement above the free surface in pressure gauge PT for the case H02. Red box: the incident waves. Green box: Interference of incident and reflected waves.

combines both these methodologies. The obtained results from this framework are validated with experimental data.

3.1. CFD model description

A two-dimensional CFD-NWT is used in this study to simulate the OWC device. The NWT is implemented in the open-source software package OpenFOAM®, using the IHFOAM framework (Higuera et al., 2013), which allows for wave generation and absorption by prescribing the boundary conditions for water levels and velocity based on a selected wave theory (in this study, both linear wave theory and Stokes' second-order theory have been used, based on the specific wave characteristics to be reproduced, as detailed in Table 1). Mass conservation and RANS equations are solved for two phases (air and water) with the interFoam solver; both phases are assumed to be incompressible. The Volume of Fluid (VOF) approach (Hirt and Nichols, 1981) is used, solving an additional transport equation for the volume phase fraction γ, which is the fraction of water per unit volume of each computational cell ($0 \leq \gamma \leq 1$, with $\gamma = 0$ and $\gamma = 1$ for the cells containing, respectively, only air or only water). For the CFD-NWT, a stabilized version of $k-\omega$ SST (Shear Stress Transport) turbulence model is used. The stabilized $k-\omega$ SST model was developed specifically to ensure a stable long-term wave propagation over relatively large domains, avoiding the exponential growth of turbulent kinetic energy density and eddy viscosity in the entire flow region under surface waves which takes place in two equations turbulence models (Larsen and Fuhrman, 2018, Fuhrman and Larsen, 2020).

As far as the numerical setup of the CFD-NWT is concerned, the PIMPLE algorithm, a hybrid between the PISO and the SIMPLE algorithms, is used for coupling pressure–velocity equations. The time step

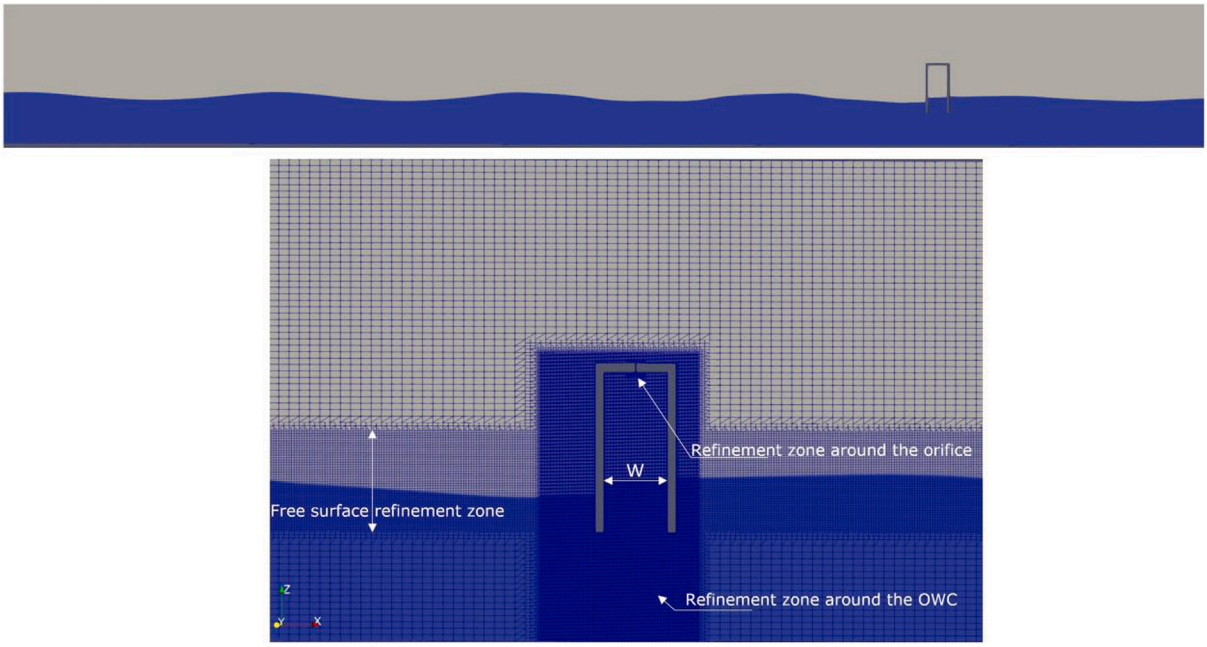

Fig. 6. Overview of the CFD-NWT (top) and of the computational mesh in the near field of the OWC (bottom).

is dynamically adjusted to maintain a Courant number Co<0.4 and a value of Co at the air–water interface αCo<0.6. Second-order accurate numerical schemes, blended with a first-order Euler scheme to improve stability, are used for the discretization of the time derivatives. Co, αCo, and the blending factor of the numerical scheme have been chosen based on sensitivity tests previously performed for a two-dimensional NWT and documented in Simonetti and Cappietti (2021). The convection term in momentum equation is discretized with a central difference interpolation scheme, while the Monotone Upwind Scheme for Scalar Conservation Laws (MUSCL) scheme is used for the convection term in the transport equation of the phase fraction γ. The Geometric-Algebraic Multi-Grid (GAMG) algorithm is used to solve the discretized equation system.

The CFD-NWT has a length of 20 m (corresponding to approximately 5–13·λ, being λ the incident wavelength). A mesh resolution of around 12 cells per wave height H is used in the free surface area (for an extension of $\pm H$ around the still water level), with a maximum aspect ratio of the cells equal to 2. The mesh in the free surface zone was chosen based on sensitivity tests aimed at ensuring mesh independence for the wave propagation in the NWT (Simonetti and Cappietti, 2021), and it is consistent with previous references in the literature (e.g. Elhanafi et al., 2016, Shalby et al., 2019, Xu and Huang, 2019). The mesh is further refined in the OWC near field 6: the length of the cell inside the OWC is ca. $W/120$ (being W the OWC chamber width). Around the slit on the top cover, the mesh has a resolution of ca. V /cells = 6 (being V = 1.7 mm the size of the slit). The NWT is composed of approximately 450.000 cells. No-slip boundary conditions are used at the bottom of the NWT and on the OWC sidewalls. The water surface is set as an atmospheric pressure boundary. Velocity components and water surface elevations at the inlet/outlet are prescribed to introduce and absorb waves with IHFOAM.

The validation of the CFD-NWT with data from laboratory experiments has been shown and discussed in Raghavan et al. (2023), showing relative errors for the height of free surface oscillation and height of the pressure oscillation inside the OWC chamber lower than 15% for all the tested wave conditions. The validation errors are also reported in Table 2 for the sake of completeness.

Table 2
Relative error between Experimental tests and CFD-NWT for the height of free surface oscillation(H_{OWC}) and height of the pressure oscillation inside the OWC chamber (∇P_{OWC}).

Case name	Relative error H_{OWC} [–]	Relative error ∇P_{OWC} [–]
H01	−0.06	0.13
H02	−0.07	0.04
H03	−0.07	0.04
H04	−0.05	0.03
H05	−0.02	0.02
H06	−0.05	−0.03
H07	−0.01	0.03
H08	0.03	0.08
H09	0.00	0.07
H10	−0.07	0.14

3.2. Numerical BEM model description

The numerical BEM model for the Box OWC device was created based on the two-body system approach, where the submerged device hull was modelled as a fixed body and the imaginary piston in place of the water column was modelled as a second body. The dimensions of the model are chosen in correspondence with the experiment. The left and right side walls of the hull were not considered since this is where the box is connected to the wave tank and is not in contact with water. There is no gap between the piston surface and the hull surface. The in-house BEM solver HAMS-MREL provides accurate results when the source and target points overlap. The imaginary piston is modelled to the length of the water column. The model is shown in Fig. 7. The hull of the body was modelled without a base, since the experimental model does not have a base as well. The piston was modelled with a base surface that is in contact with water. The input wave frequencies were considered from 2 to 5 rad/s, with the selection based on the experiments.

In order to decide on the number of elements required for discretizing the model, a convergence study was performed. The BEM solver HAMS-MREL provides the added mass coefficient, radiation damping coefficient (together characterized by the hydrodynamic coefficients) and excitation forces as the output. These parameters were utilized to perform the sensitivity analysis. The number of elements across

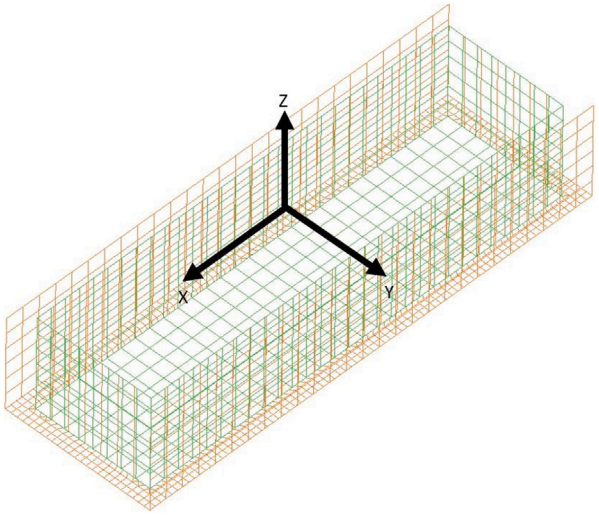

Fig. 7. HAMS-MREL model box OWC device: Box hull (orange) and imaginary piston (green). The reference global axis is XYZ.

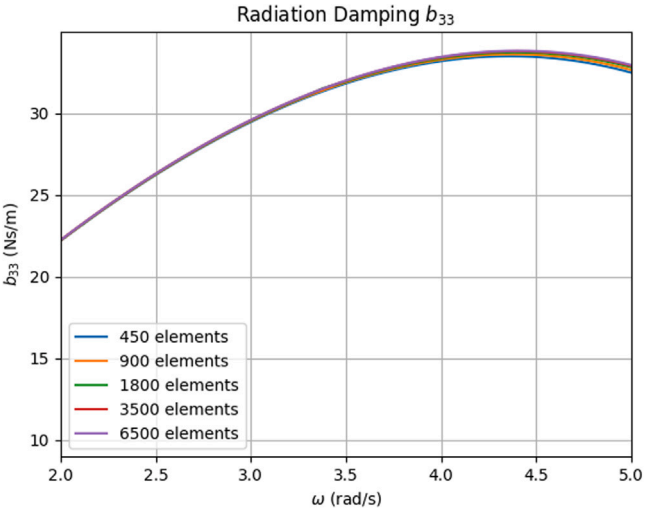

Fig. 9. Radiation damping coefficient with varying number of elements.

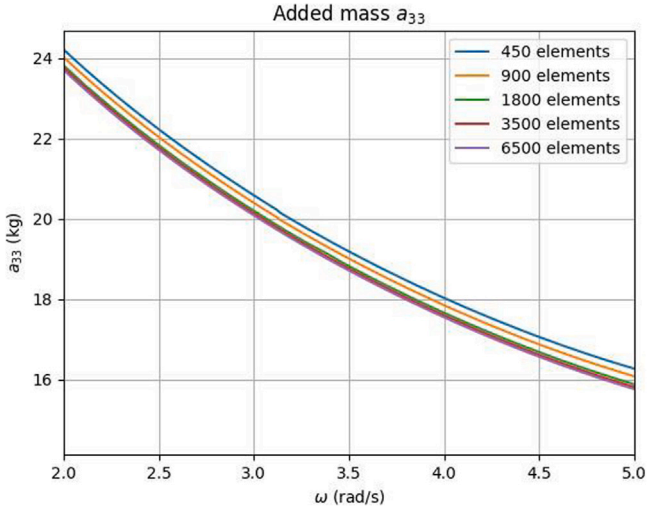

Fig. 8. Added mass coefficient with varying number of elements.

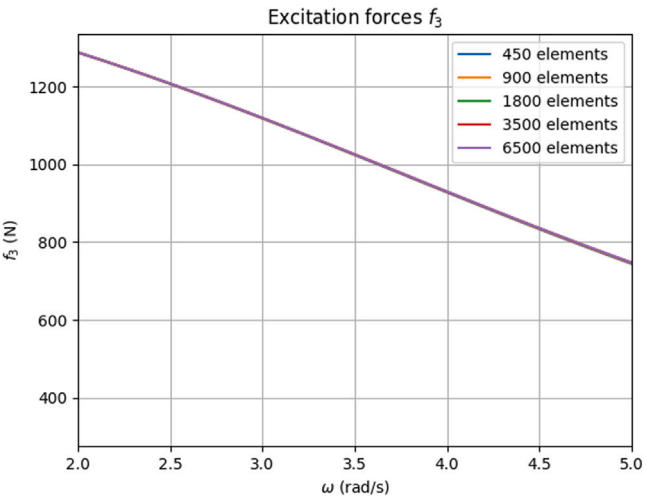

Fig. 10. Excitation force with varying number of elements.

the fixed body and piston were varied as 450, 900, 1800, 3500 and 6500 elements. The results for the added mass, radiation damping and excitation forces are shown in Figs. 8, 9 and 10 respectively.

Based on these results, 1800 elements were selected since the difference with further increase in elements was negligible (convergence is reached) for all the parameters. After obtaining the hydrodynamic coefficients and excitation forces, the dynamic equation of motion for the model can be solved to obtain the displacement of the free surface. It should be noted, that since the BEM model only considers the part of the body that is submerged in the water, the force due to the pressure above the internal free surface needs to be accounted for in another way. Therefore an additional pressure based forcing term is introduced into the final dynamic equation of motion for the device which results in Eq. (1).

$$[i\omega(m_{33}+a_{33})+b_{33}+\frac{c_{33}}{i\omega}]v_3 = f_3 - A_0 p \tag{1}$$

where ω is the radial frequency (rad/s), m_{33} is the mass of the piston (kg) which here is equal to the mass of the water column, a_{33} is the added mass of the piston (kg) obtained from HAMS-MREL, b_{33} is the radiation damping (Ns/m) obtained from HAMS-MREL, c_{33} is the hydrostatic restoring coefficient (N/m) (in this case for a box in heaving motion), v_3 is the complex amplitude of the velocity of the free surface (m/s), f_3 is the excitation force (N) obtained from HAMS-MREL and $A_0 p$ is the force due to the pressure above the free surface where A_0 is the horizontal area of the free surface (m^2) and p is the complex amplitude of the pressure (N/m^2) above the water column.

It is observed in the CFD-NWT results that the pressure above the free surface and discharge through the orifice have a non-linear relationship. However, since we are currently focusing on a linear formulation, the complex pressure amplitude p and complex heave piston velocity v_3 are related using a damping coefficient k (Sheng et al., 2014). It is assumed that the damping coefficient is real-valued and this relationship will exist only if the phase difference between the pressure and velocity is 0 or π radians. This can be written as follows:

$$p = kA_0 v_3 \tag{2}$$

In order to derive the damping coefficient relating pressure above the water column and the discharge through the orifice, two approaches are adopted based on a framework combining BEM and CFD. These are highlighted in the following section.

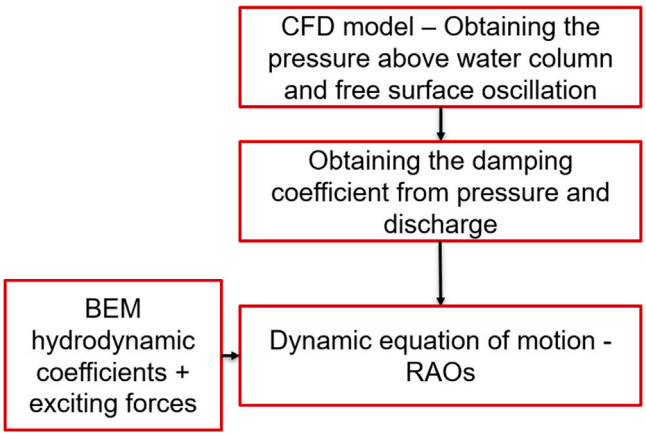

Fig. 11. Framework for combining BEM and CFD.

Table 3
Phase difference between pressure above the water column and velocity of the free surface for all 10 cases.

Case name	Phase difference ϕ [radians]
H01	0.43
H02	0.25
H03	0.27
H04	3.39
H05	3.47
H06	0.32
H07	3.38
H08	3.36
H09	0.22
H10	3.33

3.3. Framework combining BEM and CFD

This section presents the framework wherein the results from the CFD simulation can be used as input for the BEM model to derive the coefficient k. The framework is presented in Fig. 11. Using the time series of the pressure above the water column and the velocity/displacement of the free surface from the CFD analysis, the coefficient k can be derived. To illustrate the use of the coefficient relating pressure and discharge, two methods are used.

3.3.1. BEM model with coefficient considering the phase difference between pressure and discharge

As the first step to calculate the coefficient k, the time series of the pressure above the water column and displacement of the free surface obtained from the CFD simulation were used. A curve fitting was performed on the CFD free surface displacement time series (see Fig. 12) using a sine curve. The derivative of this curve was used to identify the velocity, and hence the discharge. A similar curve fitting was also performed for the CFD pressure time series (see Fig. 13). Using this, the amplitude of the pressure and velocity along with the phase difference between the two were measured.

The obtained phase difference for the 10 cases is summarized in Table 3. As observed from the table, the phase difference between the pressure and discharge is different from $0/\pi$ radians indicating that the coefficient k must be complex valued and hence characterizes stiffness and/or inertia in addition to damping (similar to Sarmento et al., 1990, Fox et al., 2021, Sheng and Aggidis, 2022, Belibassakis et al., 2020).

The obtained phase difference between the pressure and discharge is introduced into Eq. (2) to calculate the coefficient k. The parameter ϕ is introduced to represent the pressure-discharge phase difference. Then Eq. (2) thus becomes

$$k_p = (p/A_0 v_3) * \exp(i\phi) \tag{3}$$

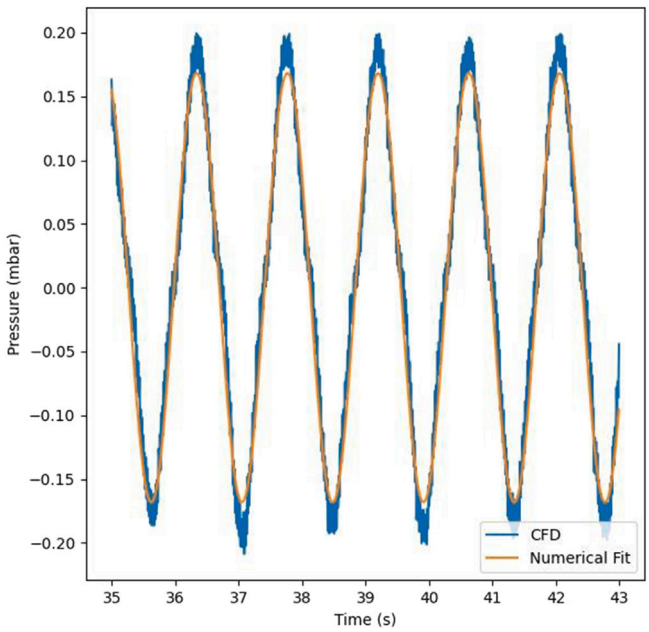

Fig. 12. Curve fitting for pressure above the free surface using CFD time series.

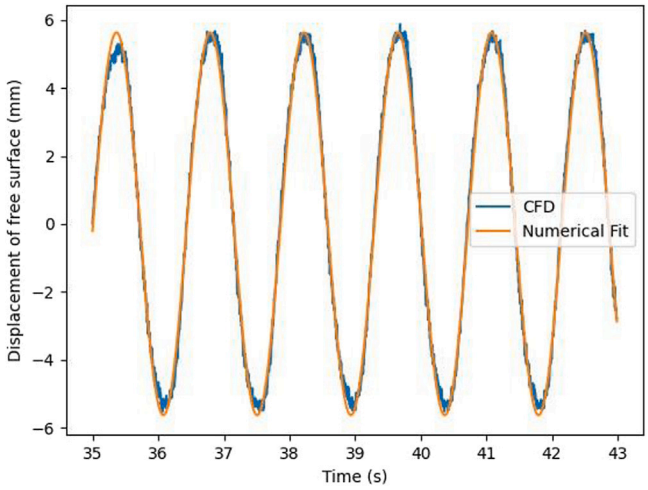

Fig. 13. Curve fitting for displacement of the free surface using CFD time series.

where k_p is the complex valued coefficient that accounts for the phase difference. It should be noted that the peak pressure and velocity values are obtained from the curve fitting process. Eq. (3) can then be substituted in Eq. (1), which will enable us to solve the dynamic equation of motion of the box OWC water column.

3.3.2. BEM model with semi-empirical frequency dependent coefficient

The second method for obtaining the coefficient k is to derive a semi-empirical frequency dependent coefficient based on curve fitting. This will be referred to as k_i to differentiate it from k_p. This was done in the following steps:

1. Based on the parameters of the BEM model i.e. the added mass coefficient (a_{33}), radiation damping coefficient (b_{33}), excitation forces (f_{33}), mass of the piston (m_{33}), restoring piston coefficient (c_{33}), and the numerical velocity (v_3) of the piston obtained from the CFD NWT, the complex value of k_i was obtained in terms of these parameters. This is shown in Eq. (4).

$$k_i = [f_3 - [i\omega(m_{33} + a_{33}) + b_{33} + \frac{c_{33}}{i\omega}]v_3]/A_0^2 v_3 \tag{4}$$

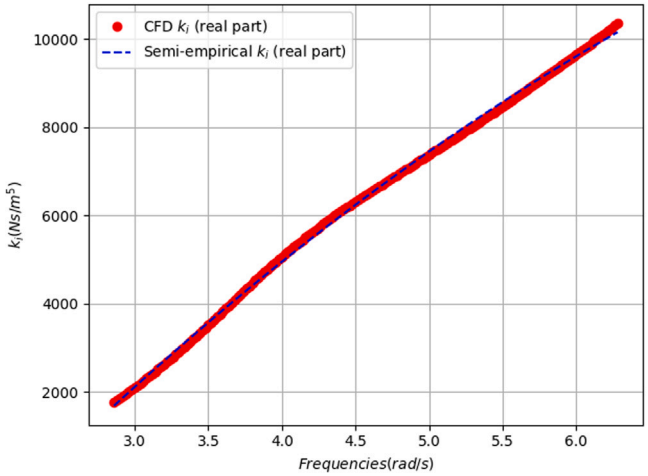

Fig. 14. Real part of the frequency dependent instantaneous coefficient k_i.

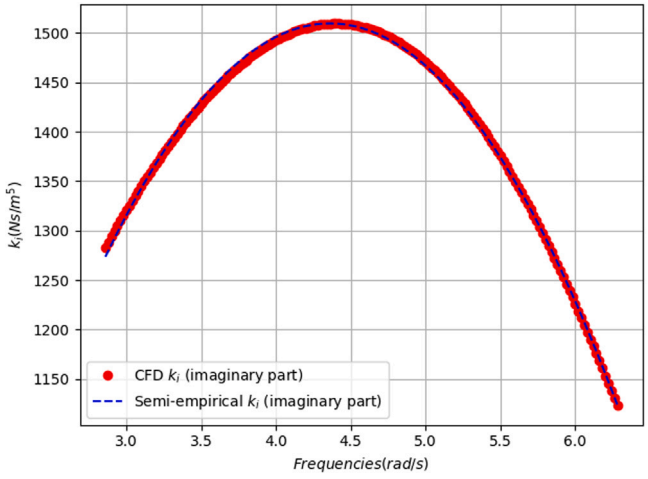

Fig. 15. Imaginary part of the frequency dependent instantaneous coefficient k_i.

2. A complex frequency dependent semi-empirical coefficient is derived. The real and imaginary parts of the complex coefficient were fitted. A curve fitting is performed with a second order polynomial of the following form:

$$k_i(\omega) = (A_1 + iA_2)\omega^2 + (B_1 + iB_2)\omega + (C_1 + iC_2) \tag{5}$$

3. The real and imaginary parts of the semi-empirical frequency dependent coefficient are shown in Figs. 14 and 15. The CFD k_i refers to the coefficient derived in step 1 using the CFD-NWT results, while the semi-empirical k_i refers to the coefficient as obtained from the curve fitting performed in step 2.

4. Results and discussion

This section discusses the main results from the study in comparing the experiments with the CFD-BEM model. To compare the developed framework model with the experiments, all wave cases were tested. Comparisons include the relative differences in the peaks of the OWC free surface oscillation, and OWC chamber pressure oscillations with respect to the experiment for the CFD-BEM model with coefficient k_p, the RAOs with both k_p and k_i, the Capture Width Ratio (CWR) with k_i as well as the coefficients k_p and k_i as obtained from the two highlighted methods in the previous section.

When considering the CFD-BEM model with k_p, the relative error of the H_{OWC} of the free surface oscillation inside the OWC can go up to 0.21 (Table 4). The relative error on the height of the pressure oscillation inside the OWC chamber, ∇P_{OWC}, varies between 0.11 to 0.20. Since the CFD-BEM is a frequency domain model, the variation of the free surface oscillation is purely sinusoidal. Hence, it is unable to capture some of the non-linear effects which could be the reasons for this difference occurring since they would directly affect the amplitude of the response.

Table 4
Relative error between Experimental tests and CFD-BEM model results (k_p) for the height of free surface oscillation (H_{OWC}) and height of the pressure oscillation inside the OWC chamber (∇P_{OWC}).

Case name	Relative error H_{OWC} [–]	Relative error ∇P_{OWC} [–]
H01	−0.04	0.15
H02	−0.11	0.17
H03	−0.10	0.15
H04	−0.21	0.16
H05	−0.02	0.20
H06	−0.01	0.16
H07	−0.06	0.16
H08	−0.05	0.14
H09	−0.04	0.11
H10	−0.02	0.12

The RAOs were computed for the two CFD-BEM cases – with k_p and k_i – using Eq. (6), in which H is the incident wave height.

$$RAO = v_3/(Hi\omega) \tag{6}$$

This is compared with the RAO obtained from CFD-NWT and experimental results. These are shown in Fig. 16. When considering the CFD-BEM model k_p, the behaviour is similar to that of the experiments, however there is a consistent overestimation by CFD-BEM model as compared to the experiments as also observed with the peak values H_{OWC}. The CFD-BEM model with k_i gives almost identical results to the experiments.

The CWR or OWC hydrodynamic efficiency is evaluated as follows based on the work of Simonetti et al. (2014):

$$CWR = \frac{\bar{P}_{BOX}}{\bar{P}_w} \tag{7}$$

where $\bar{P}_w$ is the period averaged incident wave power (W/m) and $\bar{P}_{BOX}$ is the average OWC hydrodynamic power (W/m). For evaluating $\bar{P}_w$, the incident wave characteristics corresponding to Stokes second order wave theory are considered since this is obtained for test cases H03, H05–H10 (used for evaluating the RAO), which mostly belong to Stokes second order wave theory. $\bar{P}_w$ is calculated as:

$$\bar{P}_w = \frac{1}{16}\rho g H^2 \frac{\omega}{k}\left(1 + \frac{2kh}{sinh(2kh)}\right)\left(1 + \frac{9H^2}{64k^4h^6}\right) \tag{8}$$

and $\bar{P}_{BOX}$ is evaluated as:

$$\bar{P}_{BOX} = \frac{1}{T_{OWC}} \int_{t=0}^{t=T_{OWC}} |P_t \frac{d\eta_t}{dt}|_{OWC} A_{OWC} dt \tag{9}$$

where P_t is instant pressure inside the Box model, $\frac{d\eta_t}{dt}$ is the instant OWC water surface elevation change, A_{OWC} is the OWC surface section area and T_{OWC} is the oscillation period. For calculating the CWR, the oscillation cycles selected were similar to that used for RAOs. The comparison of the CWR is shown in Fig. 17. The behaviour for both the CFD and the CFD-BEM with k_i matches well with the experiments, with the CFD-BEM model slightly under estimating the CWR. This could be resulting from the differences in the pressure estimation due to its linear nature, wherein it is hard to capture the local second/third order effects.

Fig. 18 shows the comparison of coefficients k_p and k_i. Both k_p and k_i are complex valued since they account for the phase difference between the pressure and discharge. The real part physically represents the damping and the imaginary part represents either the stiffness or inertia depending on whether they positively or negatively contribute

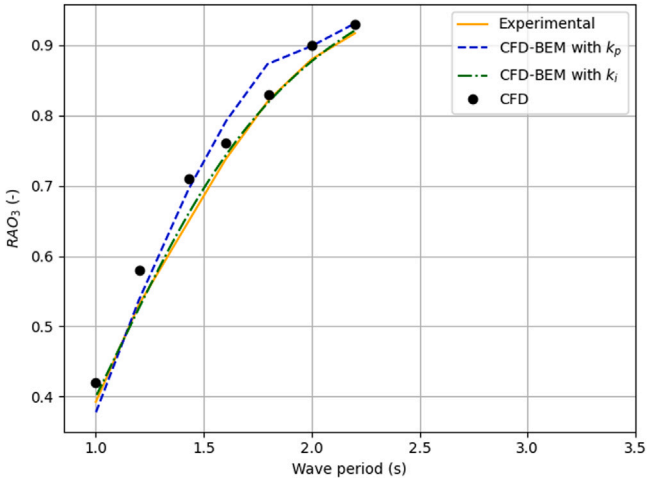

Fig. 16. Response amplitude operator (RAO) obtained with experiments, BEM and CFD modelling.

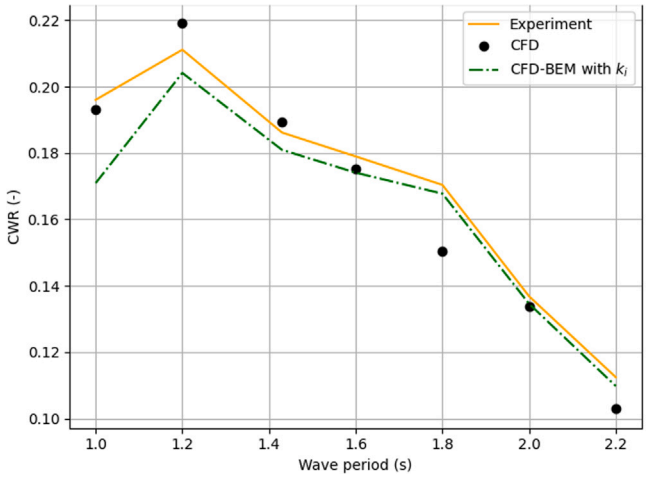

Fig. 17. Comparing CWR.

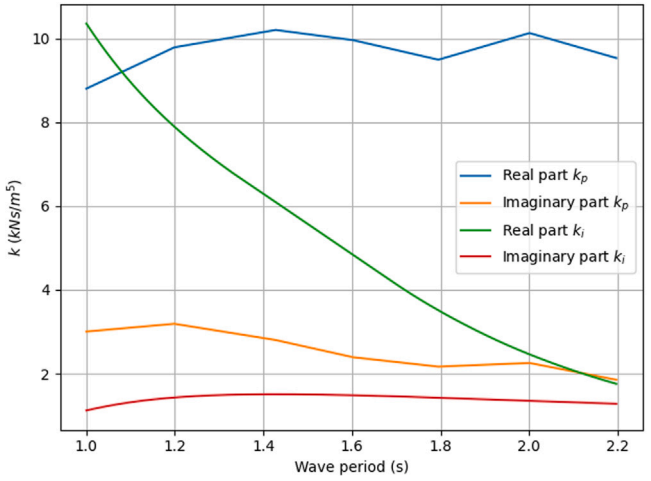

Fig. 18. Comparing k_p and k_i.

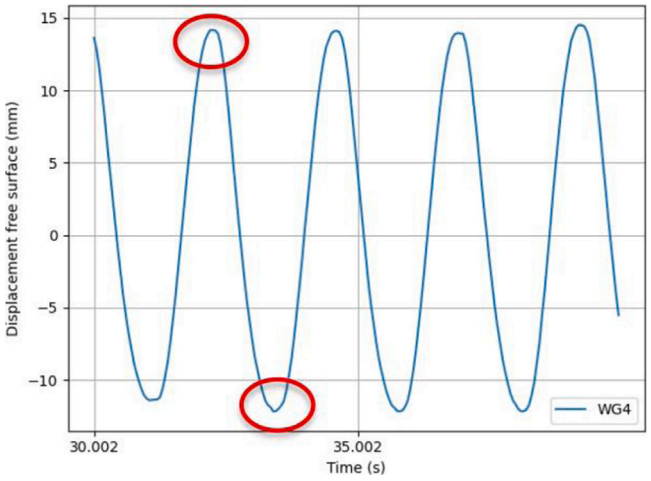

Fig. 19. H02 — Incident wave (experiment).

to the dynamic stiffness of the piston. In this case, since the imaginary part is always positive, it can be interpreted as a stiffness (restoring effect) in the linear system. Given that the experimental model here is small-scale, it is fair to assume that the effect due to air-compressibility would be negligible (Simonetti et al., 2017). Therefore, this effect could be attributed to the non-linearities introduced due to the orifice which are captured by the coefficients k_p and k_i.

Considering Fig. 18, it is observed that for the BEM model with k_i which is almost identical to the experimental results, the damping component is overestimated with increasing periods with respect to the CFD-BEM model with k_p. Similarly the spring effect is also overestimated in the k_p model. The differences could be attributed to the non-linearities which would affect the amplitude of free surface oscillation as well as the pressure above the water column, that would influence the coefficient k_p. Since the model with k_i is derived from a curve fitting process on the CFD simulations, it is expected to capture the effect of the non-linearities coming from cases considering Stoke's 2^{nd} and 3^{rd} order theories, which is not possible in the CFD-BEM model with k_p.

The non-linearities that are expected to influence the considered cases are discussed further. As an example, for the case H02, the incident wave is shown in Fig. 19.

As seen in Fig. 19, the positive and negative values are not symmetrical. The positive peak values are larger than those observed for the troughs. This behaviour is similar to that observed when ocean wave is propagating close to the shore in shallow waters.

As the water depth approaches the shallow regime, the wave shape is not sinusoidal anymore. The amplitude increases, the crest phase lasts less then half of the period while the trough is elongated and lasts more then half of the period. As the result of this transformation the wave profile becomes asymmetrical. This non-linearity observed in the CFD/experiment is not captured in the BEM numerical model. The asymmetry present in Fig. 19 is observed for all cases, however its non-linear effect can be more or less pronounced for the different cases. With increasing wave period, for the same wave height, the non-linearity increases which could be one of the reasons for the increasing deviation between the experimental and BEM results.

The asymmetry observed in Fig. 19 is also observed for the free surface oscillation (see Fig. 20) which could be due to the incident waves. Furthermore, an asymmetrical behaviour is also observed for experimental pressure variation (see Fig. 21) above the internal free surface. This clearly shows that the injection and ejection of the air above the internal free surface is different. These two aspects of the oscillation of the free surface and the pressure variation could be further contributing to the non-linearities in the system and thus the deviation between the experimental and CFD-BEM results with the k_p.

While both the proposed methods can be used for a preliminary analysis of an fixed OWC device, the CFD-BEM model with k_p can be

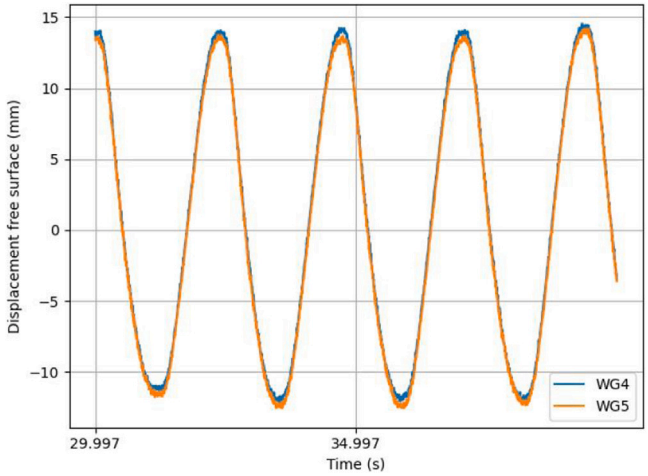

Fig. 20. H02 — Displacement of the free surface of the OWC (experiment).

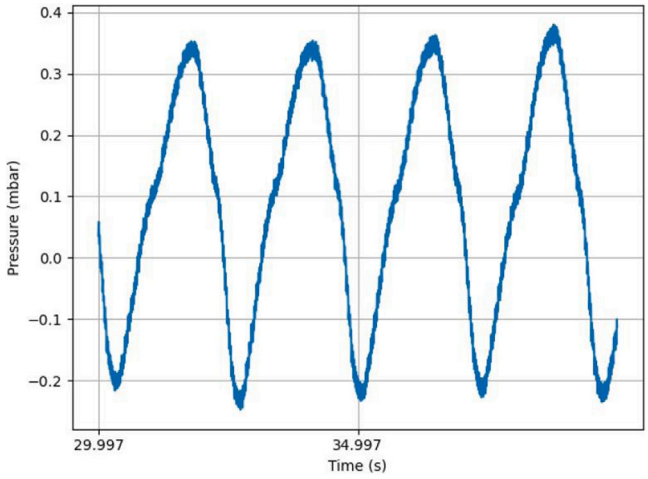

Fig. 21. H02 — Pressure variation (experiment).

used for an initial estimate of the response of the OWC, while the CFD-BEM model with k_i can be used for a more detailed analysis as in essence, it also partially accounts for the effects of the non-linearity within the linear system when considering the global behaviour of the OWC.

5. Conclusions

A new CFD-BEM framework is proposed for fixed OWC devices. The time series for the pressure above the internal water column and the displacement of the free surface of the internal water column as obtained from a non-linear CFD-NWT are combined with the hydrodynamic coefficients and excitation forces obtained from a linear BEM model(created using the in-house HAMS-MREL package) to solve the dynamic equation of motion for internal free surface of the OWC. An orifice is used to represent the PTO, which has a non-linear pressure-discharge relationship. Therefore, the proposed methodology partially captures these non-linearities and emulates them through a linear method. With this, the authors provide a framework, that is able to replace doing costly and time-consuming experiments and obtain a preliminary estimate of the response of a fixed OWC device.

As a starting point, the linear pressure discharge relationship is represented through a real-valued coefficient. Through the CFD results, it is evident that coefficient should be complex-valued due to the phase difference ϕ between pressure and discharge being different from 0 or π radians. Therefore, by evaluating and incorporating this phase difference within the dynamic equation of motion of the internal water column, the response and RAOs are derived.

To further improve the model, a complex-valued semi-empirical coefficient is derived directly from the dynamic equation of motion by substituting the added mass coefficient, radiation damping coefficient, excitation forces, mass of the water column obtained from the BEM model and calculating the response with a curve fitting procedure using the piston velocity obtained from the CFD-NWT. This coefficient partially accounts for the effects of the non-linearities within the fixed OWC that are captured by the CFD model.

From the results, it is evident that both the CFD-BEM approaches are close to the experiments. The final CFD-BEM model is closest to the experimental results as in essence, it captures all non-linearities including asymmetry in the incident wave/response/pressure curve as well as the 2^{nd} and 3^{rd} order effects in the pressure curve. Comparing the coefficients from the two CFD-BEM approaches, it is observed that the effect of non-linearities on the damping (positive real part of the coefficient) is significant with increasing wave periods, while the effect on the stiffness (positive imaginary part of the coefficient) is minor.

Going further, the authors hope to study the variations in phase difference (first CFD-BEM model) between pressure and discharge as well as the semi-empirical coefficient (second CFD-BEM model) with varying geometries (both small and large scale) as well as varying amplitudes of the incident wave, so as to provide a parametric estimate (look-up table) of the coefficient that could be directly used for a preliminary analysis of a Box OWC by using the BEM models instead of the more computationally demanding CFD models and obtaining comparable results. While the current framework is limited to small-scale models and incompressible fluids at the same small scale (air compressibility effects are currently negligible), for future work, the authors hope to incorporate scale effects and air compressibility effects within compressible CFD models that can be then transferred to BEM model through the proposed framework. Within this research, the framework considers quasi-linear/ moderate incident wave amplitudes. When considering larger amplitude incident waves, the influence of the non-linearities will have a greater effect on the phase difference between the pressure and discharge, the amplitude of the free surface oscillation and the pressure above the water column. This would significantly enhance the utility of the proposed framework.

CRediT authorship contribution statement

Vaibhav Raghavan: Writing – original draft, Visualization, Validation, Software, Methodology, Investigation, Formal analysis, Data curation. **Irene Simonetti:** Writing – original draft, Validation, Software, Methodology, Investigation, Formal analysis, Data curation, Conceptualization. **Andrei V. Metrikine:** Writing – review & editing, Supervision, Resources, Project administration, Conceptualization. **George Lavidas:** Writing – review & editing, Supervision, Resources, Project administration, Investigation, Funding acquisition, Conceptualization. **Lorenzo Cappietti:** Writing – review & editing, Supervision, Methodology, Investigation, Formal analysis, Conceptualization.

Declaration of competing interest

The authors declare the following financial interests/personal relationships which may be considered as potential competing interests: Vaibhav Raghavan reports financial support was provided by European Commission. If there are other authors, they declare that they have no known competing financial interests or personal relationships that could have appeared to influence the work reported in this paper.

Data availability

Data will be made available on request.

Acknowledgements

The authors would like to thank Andrea Esposito, who helped with creating the model and running the experiments on the Box OWC at LABIMA. The authors would also like to thank Dr. Yingyi Liu for creating HAMS. The in-house solver HAMS-MREL was built upon the HAMS solver.

This research has received funding from the European Union's Horizon 2020 research and innovation programme under grant agreement No 101006927 (VALID). The authors would also like to acknowledge SURF and access to the HPC Snellius for running the simulations in HAMS-MREL, under project EINF3290.

References

Abad, G., Lopez, J., Rodriguez, M., Marroyo, L., Iwanski, G., 2011. Doubly Fed Induction Machine: Modeling and Control for Wind Energy Generation. John Wiley & Sons.

Belibassakis, K., Magkouris, A., Rusu, E., 2020. A BEM for the hydrodynamic analysis of oscillating water column systems in variable bathymetry. Energies (ISSN: 1996-1073) 13 (13), http://dx.doi.org/10.3390/en13133403, URL https://www.mdpi.com/1996-1073/13/13/3403.

Bingham, H.B., Ducasse, D., Nielsen, K., Read, R., 2015. Hydrodynamic analysis of oscillating water column wave energy devices. Ocean Eng. Mar. Energy 1, 405–419. http://dx.doi.org/10.1007/s40722-015-0032-4, URL https://link.springer.com/article/10.1007/s40722-015-0032-4.

Carlo, L., Iuppa, C., Faraci, C., 2023. A numerical-experimental study on the hydrodynamic performance of a U-OWC wave energy converter. Renew. Energy (ISSN: 0960-1481) 203, 89–101. http://dx.doi.org/10.1016/j.renene.2022.12.057, URL https://www.sciencedirect.com/science/article/pii/S0960148122018420.

Delauré, Y., Lewis, A., 2003. 3D hydrodynamic modelling of fixed oscillating water column wave power plant by a boundary element methods. Ocean Eng. (ISSN: 0029-8018) 30 (3), 309–330. http://dx.doi.org/10.1016/S0029-8018(02)00032-X, URL https://www.sciencedirect.com/science/article/pii/S002980180200032X.

Deng, Z., Wang, C., Wang, P., Higuera, P., Wang, R., 2019. Hydrodynamic performance of an offshore-stationary OWC device with a horizontal bottom plate: Experimental and numerical study. Energy (ISSN: 0360-5442) 187, 115941. http://dx.doi.org/10.1016/j.energy.2019.115941, URL https://www.sciencedirect.com/science/article/pii/S0360544219316251.

Elhanafi, A., Fleming, A., Macfarlane, G., Leong, Z., 2016. Numerical energy balance analysis for an onshore oscillating water column–wave energy converter. Energy (ISSN: 0360-5442) 116, 539–557. http://dx.doi.org/10.1016/j.energy.2016.09.118, URL https://www.sciencedirect.com/science/article/pii/S0360544216313901.

Evans, D.V., 1978. The oscillating water column wave-energy device. IMA J. Appl. Math. (ISSN: 0272-4960) 22 (4), 423–433. http://dx.doi.org/10.1093/imamat/22.4.423.

Evans, D.V., 1982. Wave-power absorption by systems of oscillating surface pressure distributions. J. Fluid Mech. 114, 481–499. http://dx.doi.org/10.1017/S0022112082000263.

Falcão, A.F., Henriques, J.C., 2016. Oscillating-water-column wave energy converters and air turbines: A review. Renew. Energy (ISSN: 0960-1481) 85, 1391–1424. http://dx.doi.org/10.1016/j.renene.2015.07.086, URL https://www.sciencedirect.com/science/article/pii/S0960148115301828.

Falcão, A.F., Henriques, J.C., Gato, L.M., 2018. Self-rectifying air turbines for wave energy conversion: A comparative analysis. Renew. Sustain. Energy Rev. (ISSN: 1364-0321) 91, 1231–1241. http://dx.doi.org/10.1016/j.rser.2018.04.019, URL https://www.sciencedirect.com/science/article/pii/S1364032118302296.

Falcão, A.F., Henriques, J.C., Gomes, R.P., Portillo, J.C., 2022. Theoretically based correction to model test results of OWC wave energy converters to account for air compressibility effect. Renew. Energy (ISSN: 0960-1481) 198, 41–50. http://dx.doi.org/10.1016/j.renene.2022.08.034, URL https://www.sciencedirect.com/science/article/pii/S0960148122012009.

Fox, B.N., Gomes, R.P., Gato, L.M., 2021. Analysis of oscillating-water-column wave energy converter configurations for integration into caisson breakwaters. Appl. Energy (ISSN: 0306-2619) 295, 117023. http://dx.doi.org/10.1016/j.apenergy.2021.117023, URL https://www.sciencedirect.com/science/article/pii/S0306261921004876.

Fuhrman, D.R., Larsen, B.E., 2020. A discussion on "numerical computations of resonant sloshing using the modified isoadvector method and the buoyancy-modified turbulence closure model". Appl. Ocean Res. (ISSN: 0141-1187) 99, 102159. http://dx.doi.org/10.1016/j.apor.2020.102159, URL https://www.sciencedirect.com/science/article/pii/S0141118720300912.

Gaspar, L.A., Teixeira, P.R., Didier, E., 2020. Numerical analysis of the performance of two onshore oscillating water column wave energy converters at different chamber wall slopes. Ocean Eng. (ISSN: 0029-8018) 201, 107119. http://dx.doi.org/10.1016/j.oceaneng.2020.107119, URL https://www.sciencedirect.com/science/article/pii/S0029801820301840.

Higuera, P., Lara, J.L., Losada, I.J., 2013. Realistic wave generation and active wave absorption for Navier–Stokes models: Application to OpenFOAM®. Coast. Eng. (ISSN: 0378-3839) 71, 102–118. http://dx.doi.org/10.1016/j.coastaleng.2012.07.002, URL https://www.sciencedirect.com/science/article/pii/S0378383912001354.

Hirt, C.W., Nichols, B.D., 1981. Volume of fluid (VOF) method for the dynamics of free boundaries. J. Comput. Phys. 39 (1), 201–225. http://dx.doi.org/10.1016/0021-9991(81)90145-5.

Huang, Z., Huang, S., Xu, C., 2020. Characteristics of the flow around a circular OWC-type wave energy converter supported by a bottom-sitting C-shaped structure. Appl. Ocean Res. (ISSN: 0141-1187) 101, 102228. http://dx.doi.org/10.1016/j.apor.2020.102228, URL https://www.sciencedirect.com/science/article/pii/S0141118719305309.

Iturrioz, A., Guanche, R., Lara, J., Vidal, C., Losada, I., 2015. Validation of OpenFOAM® for oscillating water column three-dimensional modeling. Ocean Eng. (ISSN: 0029-8018) 107, 222–236. http://dx.doi.org/10.1016/j.oceaneng.2015.07.051, URL https://www.sciencedirect.com/science/article/pii/S0029801815003649.

Kisacik, D., Stratigaki, V., Wu, M., Cappietti, L., Simonetti, I., Troch, P., Crespo, A., Altomare, C., Domínguez, J., Hall, M., Gómez-Gesteira, M., Canelas, R.B., Stansby, P., 2020. Efficiency and survivability of a floating oscillating water column wave energy converter Moored to the seabed: An overview of the esflOWC maRINET2 database. Water (ISSN: 2073-4441) 12 (4), URL https://www.mdpi.com/2073-4441/12/4/992.

Larsen, B.E., Fuhrman, D.R., 2018. On the over-production of turbulence beneath surface waves in Reynolds-averaged Navier–Stokes models. J. Fluid Mech. 853, 419–460. http://dx.doi.org/10.1017/jfm.2018.577.

Le Méhauté, B., 1976. An Introduction to Hydrodynamics and Water Waves. Springer, http://dx.doi.org/10.1007/978-3-642-85567-2.

Liu, Y., 2019. HAMS: a frequency-domain preprocessor for wave-structure interactions–theory, development, and application. Journal of Marine Science and Engineering (ISSN: 2077-1312) 7, 81. http://dx.doi.org/10.3390/jmse7030081, URL https://www.mdpi.com/2077-1312/7/3/81.

López, I., Castro, A., Iglesias, G., 2015. Hydrodynamic performance of an oscillating water column wave energy converter by means of particle imaging velocimetry. Energy (ISSN: 0360-5442) 83, 89–103. http://dx.doi.org/10.1016/j.energy.2015.01.119, URL https://www.sciencedirect.com/science/article/pii/S0360544215002571.

Maeda, H., Santhakumar, S., Setoguchi, T., Takao, M., Kinoue, Y., Kaneko, K., 1999. Performance of an impulse turbine with fixed guide vanesfn2fn2patent pending. for wave power conversion. Renew. Energy (ISSN: 0960-1481) 17 (4), 533–547. http://dx.doi.org/10.1016/S0960-1481(98)00771-X, URL https://www.sciencedirect.com/science/article/pii/S096014819800771X.

Malara, G., Arena, F., 2013. U-oscillating water column in random waves: Modelling and performances. In: Proceedings of the International Conference on Offshore Mechanics and Arctic Engineering - OMAE, vol. 8, http://dx.doi.org/10.1115/OMAE2013-10923.

Opoku, F., Uddin, M., Atkinson, M., 2023. A review of computational methods for studying oscillating water columns – the Navier-Stokes based equation approach. Renew. Sustain. Energy Rev. (ISSN: 1364-0321) 174, 113124. http://dx.doi.org/10.1016/j.rser.2022.113124, URL https://www.sciencedirect.com/science/article/pii/S136403212201005X.

Penalba, M., Giorgi, G., Ringwood, J.V., 2017. Mathematical modelling of wave energy converters: A review of nonlinear approaches. Renew. Sustain. Energy Rev. (ISSN: 1364-0321) 78, 1188–1207. http://dx.doi.org/10.1016/j.rser.2016.11.137, URL https://www.sciencedirect.com/science/article/pii/S1364032116308784.

Raghavan, V., Esposito, A., Cappietti, L., 2022. Validation of BEM solver nemoh with experiments on a box owc device. Experiment and Numerical Validation Report NBEMB_01, LABIMA, University of Florence.

Raghavan, V., Simonetti, I., Lavidas, G., Cappietti, L., 2023. Numerical modelling of a box-type and bottom-detached oscillating water column wave energy conversion device: A comparison with experimental data and between BEM and CFD numerical modelling 15. http://dx.doi.org/10.36688/ewtec-2023-142, URL https://submissions.ewtec.org/proc-ewtec/article/view/142.

Rosati, M., Henriques, J., Ringwood, J., 2022. Oscillating-water-column wave energy converters: A critical review of numerical modelling and control. Energy Convers. Manag.: X (ISSN: 2590-1745) 16, 100322. http://dx.doi.org/10.1016/j.ecmx.2022.100322, URL https://www.sciencedirect.com/science/article/pii/S2590174522001453.

Sarmento, A., Gato, L., de O. Falcão, A., 1990. Turbine-controlled wave energy absorption by oscillating water column devices. Ocean Eng. (ISSN: 0029-8018) 17 (5), 481–497. http://dx.doi.org/10.1016/0029-8018(90)90040-D, URL https://www.sciencedirect.com/science/article/pii/002980189090040D.

Shalby, M., Elhanafi, A., Walker, P., Dorrell, D.G., 2019. CFDmodelling of a small–scale fixed multi–chamber OWC device. Appl. Ocean Res. (ISSN: 0141-1187) 88, 37–47. http://dx.doi.org/10.1016/j.apor.2019.04.003, URL https://www.sciencedirect.com/science/article/pii/S0141118718307855.

Sheng, W., Aggidis, G., 2022. Fundamentals of Wave Energy Conversions: The Dynamics of the Wave-Structure Interactions and Wave Energy Optimisation. Eliva Press, ISBN: 978-9994982769, pp. 234–235, URL https://www.elivapress.com/en/book/book-3680559883/.

Sheng, W., Alcorn, R., Lewis, A., 2014. Assessment of primary energy conversions of oscillating water columns. I. Hydrodynamic analysis. Renew. Sustain. Energy 6, http://dx.doi.org/10.1063/1.4896850, URL https://aip.scitation.org/doi/10.1063/1.4896850.

Simonetti, I., Cappietti, L., 2021. Hydraulic performance of oscillating water column structures as anti-reflection devices to reduce harbour agitation. Coast. Eng. (ISSN: 0378-3839) 165, 103837. http://dx.doi.org/10.1016/j.coastaleng.2020.103837, URL https://www.sciencedirect.com/science/article/pii/S0378383920305238.

Simonetti, I., Cappietti, L., Elsafti, H., Oumeraci, H., 2014. 3D Numerical Modelling of Oscillating Water Column Wave Energy Conversion Devices: Current Knowledge and OpenFOAM® implementation. ISBN: 978-1-138-02871-5, http://dx.doi.org/10.1201/b18973-69.

Simonetti, I., Cappietti, L., Elsafti, H., Oumeraci, H., 2017. Optimization of the geometry and the turbine induced damping for fixed detached and asymmetric OWC devices: A numerical study. Energy (ISSN: 0360-5442) 139, 1197–1209. http://dx.doi.org/10.1016/j.energy.2017.08.033, URL https://www.sciencedirect.com/science/article/pii/S0360544217314111.

Simonetti, I., Cappietti, L., Elsafti, H., Oumeraci, H., 2018. Evaluation of air compressibility effects on the performance of fixed OWC wave energy converters using CFD modelling. Renew. Energy (ISSN: 0960-1481) 119, 741–753. http://dx.doi.org/10.1016/j.renene.2017.12.027, URL https://www.sciencedirect.com/science/article/pii/S0960148117312235.

Simonetti, I., Crema, I., Cappietti, L., Elsafti, H., Oumeraci, H., 2016. Site-Specific Optimization of An OWC Wave Energy Converter in a Mediterranean Area. pp. 343–350. http://dx.doi.org/10.1201/9781315229256-43.

Sykes R.K., T.G., 2011. Predicting hydrodynamic pressure in fixed and floating owc using a piston mode. In: Proceedings of the 9th European Wave and Tidal Energy Conference.

W. Sheng, T.L., Alcorn, R., 2012. On wave energy extraction of oscillating water column device. In: 4th International Conference on Ocean Energy.

Xu, C., Huang, Z., 2019. Three-dimensional CFD simulation of a circular OWC with a nonlinear power-takeoff: Model validation and a discussion on resonant sloshing inside the pneumatic chamber. Ocean Eng. (ISSN: 0029-8018) 176, 184–198. http://dx.doi.org/10.1016/j.oceaneng.2019.02.010, URL https://www.sciencedirect.com/science/article/pii/S0029801818316160.

Zhang, Y., Zhao, Y., Sun, W., Li, J., 2021. Ocean wave energy converters: Technical principle, device realization, and performance evaluation. Renew. Sustain. Energy Rev. (ISSN: 1364-0321) 141, 110764. http://dx.doi.org/10.1016/j.rser.2021.110764, URL https://www.sciencedirect.com/science/article/pii/S1364032121000605.

Zhang, Y., Zou, Q.-P., Greaves, D., 2012. Air–water two-phase flow modelling of hydrodynamic performance of an oscillating water column device. Renew. Energy (ISSN: 0960-1481) 41, 159–170. http://dx.doi.org/10.1016/j.renene.2011.10.011, URL https://www.sciencedirect.com/science/article/pii/S0960148111005763.